JURNAL MATEMATIKA, STATISTIKA DAN KOMPUTASI e-ISSN: 2614-8811
Published by Departement of Mathematics, Hasanuddin University, Indonesia
https://journal.unhas.ac.id/index.php/jmsk/index
Vol. 23, No. 1, September 2026, pp. 246-263
DOI: 10.20956/bfpvzv53

Spectral Energy-Based Adaptive Homomorphic Filtering for Astronomical Image Enhancement

Ahmad Fawaid Ridwan[1*], Iqbal Robiyana[2]

[1] *Department of Mathematics, Faculty of Science and Technology, UIN Sunan Gunung Djati Bandung, Indonesia*
[2] *Department of Physics, Faculty of Science and Technology, UIN Sunan Gunung Djati Bandung, Indonesia*
***Email**: [*]a.fawaid.r@uinsgd.ac.id, irobiyana@uinsgd.ac.id*
**Corresponding author*
Received: 15 July 2026, revised: 5 September 2026, accepted: 7 September 2026

Abstract

Astronomical images often suffer from low contrast, uneven illumination, dark backgrounds, and sensor-induced noise, which can obscure faint celestial structures and reduce the effectiveness of subsequent image analysis. Conventional homomorphic filtering can improve illumination and contrast by attenuating low-frequency components and enhancing high-frequency details, but its use of a fixed cutoff frequency limits its adaptability to images with different spectral characteristics. This study proposes a Spectral Energy-Based Adaptive Homomorphic Filtering (SEAHF) method that estimates the cutoff frequency from the spectral energy ratio between low- and high-frequency components of each input image. The proposed mechanism modifies only the cutoff frequency while retaining the conventional Gaussian homomorphic filtering framework and fixed remaining filter parameters. The method was evaluated on 60 astronomical images from the SDSS, DECaLS, and Pan-STARRS surveys, selected from common sky coordinates available across the three sources, and compared with Contrast Limited Adaptive Histogram Equalization (CLAHE), Conventional Homomorphic Filtering (CHF), and Low-Light Image Enhancement via Illumination Map Estimation (LIME). Performance was evaluated using Structural Similarity Index Measure (SSIM), entropy, Lightness Order Error (LOE), and processing time. SEAHF consistently achieved the lowest LOE across the three datasets, with an overall LOE of 532570.5, while obtaining competitive SSIM (0.5714), entropy (6.0646), and processing time (0.009374 s). Although CLAHE and CHF achieved higher SSIM and CLAHE required less processing time, SEAHF provided the strongest illumination-order preservation while maintaining computational cost comparable to CHF. The results provide initial empirical evidence that spectral-energy-based adaptive cutoff estimation can improve illumination-order preservation while maintaining competitive structural similarity and computational cost.

Keywords: astronomical image enhancement; homomorphic filtering; spectral energy ratio; adaptive cutoff frequency

1. INTRODUCTION

Image enhancement aims to improve the visual quality and information content of digital images, enabling more reliable interpretation by both human observers and computer vision systems. In astronomical imaging, enhancement plays a crucial role because celestial objects such as galaxies, nebulae, and faint stars are often captured under challenging acquisition conditions. Astronomical images commonly exhibit low contrast, uneven illumination, dark backgrounds, and sensor-induced noise, which reduce the visibility of important structural details and limit subsequent scientific analysis [8], [11], [14], [15], [20].

Image enhancement aims to improve the visual quality and information content of digital images, enabling more reliable interpretation by both human observers and computer vision systems. In astronomical imaging, enhancement plays a crucial role because celestial objects such as galaxies, nebulae, and faint stars are often captured under challenging acquisition conditions. Astronomical images commonly exhibit low contrast, uneven illumination, dark backgrounds, and sensor-induced noise, which reduce the visibility of important structural details and limit subsequent scientific analysis [8], [11], [14], [15], [20].

Recent large-scale astronomical surveys, including the Sloan Digital Sky Survey (SDSS) [1], Dark Energy Camera Legacy Survey (DECaLS) [3], and Pan-STARRS [2], have produced extensive collections of publicly available high-resolution astronomical images. Although these datasets provide valuable observational resources, many images still contain faint objects with limited contrast, making image enhancement an essential preprocessing step before further analysis [8], [15].

Image enhancement methods have been extensively developed in both the spatial and frequency domains. Among frequency-domain techniques, homomorphic filtering remains attractive because it separates illumination and reflectance components, allowing simultaneous illumination normalization and contrast enhancement [6]. By attenuating low-frequency illumination components while amplifying high-frequency detail components in the Fourier domain, homomorphic filtering is well suited for astronomical images, whose spectra are typically dominated by low-frequency background information. The effectiveness of homomorphic filtering therefore depends, in part, on how the frequency components are separated and how the transition between attenuated and amplified frequency regions is controlled.

Recent advances in image enhancement have increasingly relied on deep learning approaches, including convolutional neural networks, diffusion models, and frequency-aware learning techniques [10], [17], [19], [20], [21], [23]. Similar approaches have also been applied to astronomical image enhancement, reconstruction, and super-resolution [14], [15]. Despite their strong performance, these methods generally require large training datasets, complex optimization procedures, and substantial computational resources, limiting their practicality in settings where a lightweight and training-free enhancement approach is preferred.

Consequently, frequency-domain enhancement remains an active research area due to its relatively low computational complexity and ability to preserve structural information [12], [17]. Homomorphic filtering has been successfully applied to various applications, including thin-cloud removal in remote sensing [12], active laser image enhancement [5], illumination normalization for face recognition [4], and adaptive filtering for simultaneous illumination correction and noise suppression [13]. However, conventional homomorphic filtering generally employs a fixed cutoff frequency, which cannot adequately accommodate variations in image spectral characteristics. This limitation becomes more significant in astronomical images, where spectral distributions vary considerably according to object type, brightness level, and acquisition conditions [8], [11], [14], [15], [20].

Previous studies have also explored adaptive variants of homomorphic filtering for different image-processing applications. For example, Fan et al. developed an adaptive homomorphic filtering approach combined with total variation for laser imaging [5], while Liu proposed a self-adaptive filtering strategy combined with homomorphic filtering for image enhancement [13]. These studies demonstrate that adapting the filtering process to image characteristics can improve the flexibility of conventional homomorphic filtering. However, the adaptation mechanisms are generally designed according to the requirements of their respective applications. In the context of astronomical image enhancement, the use of a descriptor derived directly from the spectral energy distribution to determine the cutoff frequency remains relatively unexplored.

Spectral energy distribution provides useful information regarding the dominance of low- and high-frequency components in an image [9]. Because the cutoff frequency determines the separation between frequency components that are predominantly attenuated and those that are increasingly amplified, the relative distribution of spectral energy provides a direct image-dependent characteristic that can be used to guide cutoff selection [6]. A normalized spectral energy ratio is therefore considered in this study as a simple descriptor of the relative dominance of high-frequency information. This choice is motivated primarily by its direct relationship to the frequency content of the input image and by the possibility of incorporating it into the conventional homomorphic filtering framework without substantially increasing computational complexity. The resulting relationship between spectral energy ratio and cutoff frequency is treated as a practical design choice for image-dependent adaptation, rather than as an analytically optimal mapping. The use of spectral energy characteristics as a direct criterion for cutoff estimation has therefore been investigated here as an initial, computationally lightweight adaptive strategy rather than as a claim that spectral energy is a universally optimal descriptor.

Based on this consideration, a research gap remains in developing and evaluating a simple image-dependent mechanism that directly links the spectral characteristics of an astronomical image to the cutoff frequency of homomorphic filtering while retaining the simplicity of the conventional framework. Such a mechanism is particularly relevant for an initial evaluation on heterogeneous astronomical images, where the spectral distribution may differ between observations and a single fixed cutoff may not provide the same enhancement behavior for all inputs.

Therefore, this study proposes an Spectral Energy-Based Adaptive Homomorphic Filtering (SEAHF) method that automatically determines the cutoff frequency based on spectral energy analysis. The proposed mechanism specifically adapts the cutoff frequency to the spectral characteristics of each input image, while the remaining homomorphic filter parameters are kept fixed. In this way, SEAHF retains the conventional homomorphic filtering framework while introducing an image-dependent cutoff selection mechanism. The proposed method is evaluated using publicly available astronomical datasets from SDSS [1], DECaLS [3], and Pan-STARRS [2], and compared with Contrast Limited Adaptive Histogram Equalization (CLAHE), Conventional Homomorphic Filtering (CHF), and Low-Light Image Enhancement via Illumination Map Estimation (LIME) [7]. Performance is assessed using Structural Similarity Index Measure (SSIM) [18], Lightness Order Error (LOE), entropy, and processing time to evaluate structural preservation, illumination consistency, information content, and computational efficiency. The evaluation is intended to examine the trade-off among these performance aspects and to provide an initial assessment of the applicability of spectral-energy-based adaptive cutoff estimation to astronomical image enhancement.

2. METHODS

2.1. Proposed Method

This study proposes an Spectral Energy-Based Adaptive Homomorphic Filtering (SEAHF) method for enhancing low-contrast astronomical images. Unlike conventional homomorphic filtering, which employs a fixed cutoff frequency, the proposed method determines the cutoff frequency adaptively from the spectral energy distribution of each input image. The adaptive mechanism is applied only to the cutoff frequency, while the remaining homomorphic filter parameters are kept fixed throughout the experiments. This design enables the enhancement process to accommodate variations in the frequency characteristics of individual astronomical images while retaining the conventional homomorphic filtering framework.

The proposed framework consists of the following steps: (1) input astronomical image, (2) image preprocessing, (3) logarithmic transformation, (4) two-dimensional Fourier transform, (5) spectral energy analysis, (6) adaptive cutoff frequency estimation, (7) homomorphic filtering, (8) inverse Fourier transform, (9) image reconstruction, and (10) performance evaluation. Among these steps, spectral energy analysis and adaptive cutoff frequency estimation constitute the adaptive component of SEAHF, whereas the subsequent filtering operation follows the conventional Gaussian homomorphic filtering framework. The complete workflow of the proposed SEAHF is illustrated in Figure 2.1.

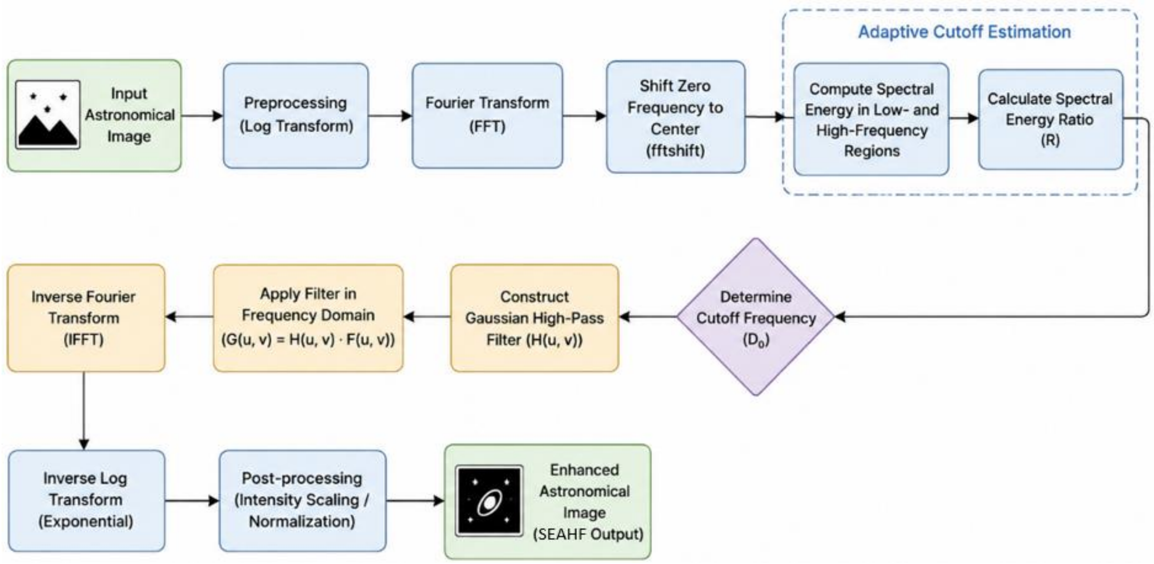

Figure 2.1. Workflow of SEAHF for Astronomical Image

Homomorphic filtering was selected because it effectively separates illumination and reflectance components in the frequency domain, allowing simultaneous illumination normalization and contrast enhancement [6]. Previous studies have demonstrated its effectiveness in remote sensing [12], laser imaging [5], face recognition [4], and adaptive image enhancement [13]. However, most existing implementations employ a fixed cutoff frequency that cannot adequately accommodate the diverse spectral characteristics of astronomical images [8], [11], [14], [15], [20].

To address this limitation, SEAHF introduces an image-dependent cutoff estimation step based on spectral energy analysis before the homomorphic filtering operation. The spectral characteristics of each input image are first quantified, and the resulting spectral energy ratio is subsequently used to determine the cutoff frequency within predefined bounds. This preserves the original filtering formulation while allowing the cutoff frequency to vary between input images. The enhanced images are evaluated using Structural Similarity Index Measure (SSIM), Lightness Order Error (LOE), entropy, and processing time. Performance is compared with Contrast Limited Adaptive Histogram Equalization (CLAHE), Conventional Homomorphic Filtering (CHF), and Low-Light Image Enhancement via Illumination Map Estimation (LIME) [7].

2.2. Astronomical Image Dataset

Experiments were conducted using publicly available astronomical images collected from three large-scale sky surveys: the Sloan Digital Sky Survey (SDSS) [1], Dark Energy Camera Legacy Survey (DECaLS) [3], and Pan-STARRS [2]. The sampling process started from a list of astronomical objects obtained from the SDSS DR18 dataset. The corresponding sky coordinates were then cross-checked against the DECaLS and Pan-STARRS surveys to determine whether image data were available at the same positions. Coordinates without corresponding image availability in either of the two other surveys were excluded. From the remaining common sky positions, 20 coordinates were selected for the experimental dataset, resulting in 20 images from each survey and 60 images in total.

The dataset consists primarily of galaxy images with varying brightness levels and contrast conditions. Such images typically exhibit faint structures embedded in dark backgrounds, representing challenging cases for image enhancement because important structural information is often difficult to observe without preprocessing. The selected galaxy images were used as an initial test case for evaluating the proposed spectral-energy-based adaptive cutoff mechanism rather than as a comprehensive representation of all astronomical object types available in the three surveys.

For image acquisition, SDSS images were obtained using the SkyServer DR18 Image Cutout service with a scale of 0.2 arcsec/pixel and an image size of 256 × 256 pixels. DECaLS images were obtained from Legacy Survey DR10 with a pixel scale of 0.262 arcsec/pixel and an image size of 256 × 256 pixels. Pan-STARRS images were obtained using the corresponding sky coordinates with an image size of 256 × 256 pixels and combined g, r, and i bands to produce RGB images.

Before enhancement, all images were converted to grayscale and normalized to the intensity range of [0,1]. Because the retrieved images were already generated at 256 × 256 pixels, no additional resizing was required during preprocessing. Grayscale conversion allows the proposed method to focus on intensity distribution and spectral characteristics without introducing color-related variations. The same preprocessing procedure was applied to the input images used by SEAHF and all comparison methods.

The use of common sky coordinates provides a consistent basis for comparing image enhancement results across the three survey sources, while the identical image dimensions and common preprocessing procedure ensure consistent input conditions for all enhancement methods. Nevertheless, the experimental dataset is limited to 60 selected galaxy images and should therefore be regarded as an initial evaluation rather than a comprehensive assessment of the method's generalization across different astronomical object types and observational conditions.

2.3. Fourier Transform and Spectral Energy Analysis

Spectral energy analysis is employed to characterize the frequency distribution of astronomical images and serves as the basis for estimating the adaptive cutoff frequency. Since astronomical images are generally dominated by low-frequency background illumination with relatively weak high-frequency object details, spectral energy provides an effective representation of image characteristics for adaptive frequency-domain enhancement [9].

After preprocessing, the input image is transformed into the frequency domain using the two-dimensional Fast Fourier Transform (FFT):

$$F(u,v)=\sum_{x=0}^{M-1}\sum_{y=0}^{N-1} f(x,y)e^{-j2\pi\left(\frac{ux}{M}+\frac{vy}{N}\right)} \tag{2.1}$$

where $f(x,y)$ denotes the input image, $F(u,v)$ represents its frequency-domain representation, and M and N are the image dimensions.

To facilitate frequency analysis, the Fourier spectrum is shifted so that the zero-frequency component is located at the center of the spectrum. The corresponding magnitude spectrum is computed as

$$S(u,v) = |F(u,v)| \tag{2.2}$$

The spectral energy at each frequency component is then calculated as

$$E(u,v) = |F(u,v)|^2 \tag{2.3}$$

where $E(u, v)$ represents the spectral energy associated with the frequency coordinate (u, v). Thus, the energy is proportional to the squared magnitude of the corresponding Fourier coefficient, providing a direct measure of the contribution of each frequency component to the overall spectrum.

The total spectral energy is obtained by summing the energy over all frequency components

$$E_{total} = \sum_{u=0}^{M-1} \sum_{v=0}^{N-1} |F(u,v)|^2 \tag{2.4}$$

The total energy provides the reference quantity for describing the relative distribution of spectral energy across the frequency domain. Because the proposed adaptive mechanism is based on the relative rather than the absolute spectral content, the energy components are subsequently partitioned into low- and high-frequency regions.

To distinguish low and high-frequency components, the radial distance of each frequency component from the spectrum center is calculated as

$$D(u,v) = \sqrt{(u-u_c)^2 + (v-v_c)^2} \tag{2.5}$$

where (u_c, v_c) denotes the center of the shifted Fourier spectrum.

The radial distance provides a frequency-domain coordinate for grouping spectral components according to their distance from the zero-frequency location. Components closer to the spectrum center correspond to lower spatial frequencies, whereas components farther from the center represent higher spatial frequencies. The spectral energy can therefore be summarized according to its radial distribution in the Fourier domain.

In this study, the median radial distance is used as the boundary between the low- and high-frequency regions. The median is selected as a simple and parameter-independent partition criterion, avoiding the introduction of an additional empirically tuned frequency threshold. Consequently, the frequency partition is determined directly from the radial distribution of each input spectrum. This selection is intended as a practical initial partitioning rule for the proposed adaptive mechanism rather than as a claim that the median represents an optimal frequency boundary.

The low-frequency energy is computed as

$$E_L = \sum_{D(u,v) \leq D_m} |F(u,v)|^2 \tag{2.6}$$

where E_L represents the accumulated energy inside the low-frequency region. Similarly, the high-frequency energy is calculated by

$$E_H = \sum_{D(u,v) > D_m} |F(u,v)|^2 \tag{2.7}$$

where E_H denotes the accumulated energy outside the threshold radius. The resulting low- and high-frequency energies describe how the total spectral energy is distributed between the two regions. These quantities are subsequently used to construct a normalized spectral energy ratio for image-dependent cutoff estimation, as described in the following subsection.

2.4. Adaptive Cutoff Frequency

Unlike conventional homomorphic filtering, which employs a fixed cutoff frequency for all images, the proposed method estimates the cutoff frequency adaptively according to the spectral energy distribution of each astronomical image. Since astronomical images exhibit different object brightness, background illumination, and spectral characteristics, using a fixed cutoff frequency may lead to either insufficient enhancement or excessive amplification of image details [8], [11], [14], [15], [20].

To characterize the spectral distribution, the Fourier spectrum is divided into low-frequency and high-frequency regions using the median radial distance obtained in Section 2.3. The low- and high-frequency energies obtained from this partition, E_L and E_H, are used to describe the relative distribution of spectral energy in each input image. The spectral energy ratio is then defined as

$$R = \frac{E_H}{E_L + E_H}. \tag{2.8}$$

The ratio Rrepresents the proportion of spectral energy located in the high-frequency region relative to the total spectral energy represented by the two regions. Since $E_L \geq 0$ and $E_H \geq 0$, R is bounded within $0 \leq R \leq 1$ when $E_L + E_H > 0$. A smaller value of R indicates that the spectrum is relatively dominated by low-frequency components, whereas a larger value indicates a greater relative contribution from high-frequency components.

The normalized ratio is used to characterize the relative spectral composition of each input image rather than its absolute energy magnitude. Based on this characterization, images with relatively weak high-frequency content are associated with smaller values of R, whereas images with relatively stronger high-frequency content produce larger values of R.

The relationship between R and the cutoff frequency is motivated by the role of D_0 in the Gaussian homomorphic filter. A smaller R indicates that a larger proportion of the image energy is concentrated in the low-frequency region. In this case, a larger cutoff frequency is used to shift the filter transition toward higher frequencies, allowing a broader range of frequency components to remain under the low-frequency attenuation regime before the high-frequency amplification becomes dominant. Conversely, when R is larger, the image already contains a relatively greater proportion of high-frequency information; therefore, a smaller cutoff frequency is used so that the transition toward high-frequency enhancement occurs earlier. This inverse relationship provides the conceptual basis for adapting D_0 to the spectral characteristics of each input image.

Based on this consideration, the spectral energy ratio is used to determine the cutoff frequency within a predefined range. A smaller spectral energy ratio is mapped to a larger cutoff frequency, while a larger spectral energy ratio is mapped to a smaller cutoff frequency. The adaptive cutoff frequency is determined using

$$D_0 = D_{min} + (D_{max} - D_{min})(1 - R) \tag{2.9}$$

where D_{min} and D_{max} denote the lower and upper bounds of the cutoff frequency, respectively.

The linear mapping in (2.9) provides a simple deterministic relationship between the normalized spectral energy ratio and the cutoff frequency. The mapping preserves the intended monotonic inverse relationship and constrains the resulting cutoff frequency to the predefined interval $[D_{\min}, D_{\max}]$. In particular, $R = 0$ results in $D_0 = D_{\max}$, whereas $R = 1$ results in $D_0 = D_{\min}$.

The monotonic behavior of the mapping follows directly from

$$\frac{dD_0}{dR} = -(D_{\max} - D_{\min}) \leq 0. \tag{2.10}$$

Therefore, an increase in the relative high-frequency energy produces a non-increasing cutoff frequency, while a decrease in the high-frequency energy ratio produces a non-decreasing cutoff frequency.

The linear relationship in (2.9) is adopted as a heuristic design choice for this initial implementation. It is intended to provide a simple and bounded mapping without introducing additional parameters associated with the shape of a nonlinear function, rather than to represent a theoretically optimal relationship between spectral energy distribution and cutoff frequency. Alternative mapping functions and their sensitivity to enhancement performance are beyond the scope of the present study.

The estimated adaptive cutoff frequency is subsequently employed in the proposed Spectral Energy-Based Adaptive Homomorphic Filtering described in the following subsection.

2.5. Spectral Energy-Based Adaptive Homomorphic Filtering

After estimating the adaptive cutoff frequency in Section 2.4, the Spectral Energy-Based Adaptive Homomorphic Filtering (SEAHF) is applied to enhance the astronomical images in the frequency domain. The adaptive mechanism modifies only the cutoff frequency D_0, while the formulation of the Gaussian homomorphic filter and its other parameters remains unchanged.

Similar to conventional homomorphic filtering, the input image is modeled as the product of an illumination component and a reflectance component:

$$f(x, y) = i(x, y) \,.\, r(x, y) \tag{2.11}$$

where $f(x, y)$ denotes the input image, $i(x, y)$ represents the illumination component, and $r(x, y)$ denotes the reflectance component.

To transform the multiplicative relationship into an additive form, a logarithmic transformation is applied:

$$z(x, y) = \ln\big(1 + f(x, y)\big) \tag{2.12}$$

where $z(x, y)$ denotes the logarithmically transformed image. The $1 +$ term corresponds to the *log1p* operation used in the implementation and ensures that the logarithmic transformation can be applied to normalized image intensities including zero.

The transformed image is then converted into the frequency domain using the Fourier transform:

$$Z(u, v) = \mathcal{F}\{z(x, y)\} \tag{2.13}$$

where $Z(u, v)$ denotes the Fourier-domain representation of the logarithmically transformed image.

The enhancement is performed using a Gaussian high-pass homomorphic filter defined as

$$H(u, v) = (\gamma_H - \gamma_L)\left(1 - e^{-c\frac{D(u,v)^2}{D_0^2}}\right) + \gamma_L \tag{2.14}$$

where γ_H and γ_L are the gains for the high- and low-frequency components, respectively, c controls the slope of the filter response, $D(u, v)$ denotes the radial distance from the center of the Fourier spectrum, and D_0 denotes the adaptive cutoff frequency obtained from (2.9).

The cutoff frequency D_0 controls the transition of the Gaussian filter response across the frequency domain. A larger value of D_0 shifts the transition toward higher radial frequencies, whereas a smaller value causes the transition to occur at lower radial frequencies. Consequently, the image-dependent value of D_0 determines the frequency range affected by the homomorphic enhancement, while the remaining filter parameters are kept fixed.

The filtered spectrum is computed as

$$G(u,v) = H(u,v) \,.\, Z(u,v) \tag{2.15}$$

where $G(u, v)$denotes the filtered frequency-domain representation.

After filtering, the enhanced image is reconstructed through the inverse Fourier transform followed by the inverse of the logarithmic transformation:

$$g(x,y) = \exp(\mathcal{F}^{-1}\{G(u,v)\}) \tag{2.16}$$

where $g(x, y)$ denotes the reconstructed enhanced image. The exponential operation reverses the logarithmic transformation applied in (2.12), returning the filtered result to the image-intensity domain.

For all experiments, the homomorphic filter parameters were set to $\gamma_L = 0.5$, $\gamma_H = 2.0$, and $c = 1.0$. The adaptive cutoff frequency was constrained by $D_{\min} = 15$ and $D_{\max} = 60$ pixels. Consequently, only D_0 varies between input images according to their spectral characteristics, whereas γ_L, γ_H, c, $D_{\min}$, and $D_{\max}$ remain fixed throughout the experiments.

For comparison, Conventional Homomorphic Filtering (CHF) used the same values of $\gamma_L = 0.5$, $\gamma_H = 2.0$, and $c = 1.0$, with a fixed cutoff frequency of $D_0 = 30$ pixels. Thus, the principal difference between CHF and SEAHF is the cutoff-frequency selection mechanism, with CHF using a fixed value and SEAHF determining D_0adaptively from the spectral energy ratio. This configuration preserves the Gaussian homomorphic filtering framework while introducing image-dependent cutoff selection as the adaptive component of SEAHF.

2.6. Performance Evaluation

The proposed SEAHF method was evaluated quantitatively using four complementary performance metrics: Structural Similarity Index Measure (SSIM), entropy, Lightness Order Error (LOE), and processing time. These metrics were selected to assess structural preservation, information content, illumination consistency, and computational efficiency, respectively.

Structural preservation was evaluated using the Structural Similarity Index Measure (SSIM), which measures the similarity between the original and enhanced images by considering luminance, contrast, and structural information [18]. The SSIM is defined as

$$SSIM(x,y) = \frac{(2\mu_x\mu_y + C_1)(2\sigma_{xy} + C_2)}{(\mu_x^2 + \mu_y^2 C_1)(\sigma_x^2 + \sigma_y^2 + C_2)} \tag{2.17}$$

where μ_x and μ_y denote the mean intensities, σ_x^2 and σ_y^2 represent the variances, σ_{xy} is the covariance, and C_1 and C_2 are stabilization constants.

Image information content was measured using Shannon Entropy,

$$H = -\sum_{i=0}^{L-1} p(i)\log_2 p(i) \tag{2.18}$$

where $p(i)$ denotes the probability of intensity level i, and L is the number of gray levels. Higher entropy generally indicates a richer intensity distribution.

Illumination preservation was evaluated using Lightness Order Error (LOE), which quantifies the consistency of relative lightness ordering between the original and enhanced images.

$$LOE = \frac{1}{MN}\sum_{x=1}^{M}\sum_{y=1}^{N} RD(x,y) \tag{2.19}$$

where $RD(x,y)$ denote the local lightness order difference is calculated between the original and enhanced images. Lower LOE indicates better preservation of the original illumination relationship [17].

In addition to image quality metrics, computational efficiency was evaluated by measuring the average processing time required to enhance a single image. The execution time was measured only during the enhancement stage, excluding image loading and preprocessing, so that the computational cost of the enhancement algorithms could be compared under the same input conditions. The processing time for each image was recorded during the enhancement stage, and the reported values represent the average processing time across the evaluated images. All experiments were implemented in Python and executed using Google Colaboratory. The reported computational time was measured within the corresponding Colab runtime. The implementation used NumPy, OpenCV, Pandas, and scikit-image for numerical computation, image processing, data handling, and image-quality evaluation, respectively.

The evaluation was conducted on 60 astronomical images comprising 20 common sky positions from each of the SDSS, DECaLS, and Pan-STARRS datasets. The same input images and preprocessing procedure were used for all enhancement methods. SEAHF was compared with Contrast Limited Adaptive Histogram Equalization (CLAHE), Conventional Homomorphic Filtering (CHF), and Low-Light Image Enhancement via Illumination Map Estimation (LIME).

For SEAHF, the cutoff frequency was determined independently for each input image using the spectral energy ratio described in Section 2.4, whereas CHF used a fixed cutoff frequency of 30 pixels. The remaining homomorphic filter parameters were kept identical between SEAHF and CHF. This configuration isolates the effect of the adaptive cutoff-frequency mechanism in the comparison between the two homomorphic filtering approaches.

For each metric, the reported values represent the average performance over the evaluated images within each dataset and over the complete 60-image collection. The evaluation therefore focuses on comparative average performance rather than statistical significance testing across methods.

3. RESULTS AND DISCUSSION

3.1. Spectral Analysis of Adaptive Fourier-Domain Homomorphic Filter

To further investigate the behavior of the proposed method, the Fourier magnitude spectra before and after frequency-domain filtering were analyzed. Figure 3.1 illustrates representative spectra from the SDSS, DECaLS, and Pan-STARRS datasets.

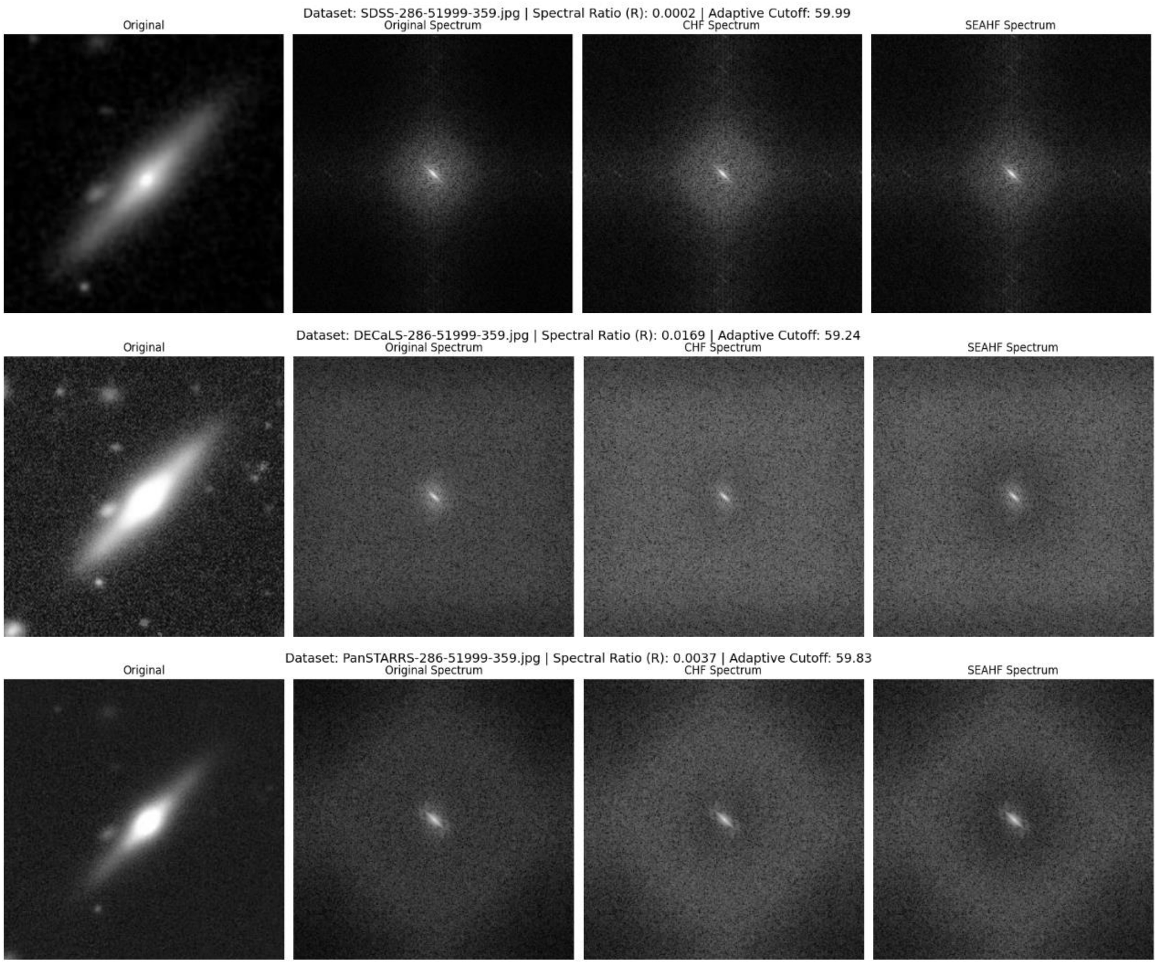

Figure 3.1. Representative spectra from the SDSS, DECaLS, and Pan-STARRS datasets.

As shown in Figure 3.1, the spectral energy of the astronomical images is primarily concentrated around the center of the Fourier spectrum, indicating a dominant contribution from low-frequency components. These components are associated mainly with slowly varying image intensity structures, including the background illumination and broad-scale structures of the observed galaxies, whereas higher-frequency components are distributed farther from the spectrum center and correspond to finer spatial variations.

Unlike conventional homomorphic filtering, which applies a fixed cutoff frequency to every image, SEAHF estimates the cutoff frequency from the spectral energy ratio. The representative images produced spectral ratios of 0.0002, 0.0169, and 0.0037 for the SDSS, DECaLS, and Pan-STARRS datasets, resulting in adaptive cutoff frequencies of 59.99, 59.24, and 59.83 pixels, respectively. These values follow the inverse monotonic relationship defined in Eq. (2.9): the representative image with the largest high-frequency energy ratio ($R = 0.0169$) receives the smallest cutoff frequency ($D_0 = 59.24$), whereas the image with the smallest ratio ($R = 0.0002$) receives the largest cutoff frequency ($D_0 = 59.99$). This confirms that the cutoff estimation responds consistently to differences in the relative spectral composition of the input images.

The cutoff values in these representative examples are relatively close to the upper bound of 60 pixels. This indicates that the selected astronomical images are predominantly characterized by low-frequency spectral energy, with only a relatively small proportion of energy located in the high-frequency region. Nevertheless, the adaptive mechanism still preserves the intended image-dependent variation in D_0 rather than imposing a single cutoff value on all images. The relatively narrow range of D_0in these examples also indicates that the degree of adaptation is influenced by the spectral characteristics of the selected dataset, rather than being uniformly distributed across the predefined cutoff range.

Although the filtered spectra generated by CHF and SEAHF exhibit similar overall distributions, the two methods differ in how the cutoff frequency is determined. CHF applies the same fixed cutoff to every image, whereas SEAHF uses the spectral energy ratio to determine D_0independently for each input image. As a result, the overall filtering framework remains similar, while the transition of the filter response can vary according to the spectral characteristics of the input image.

The spectral analysis therefore provides direct evidence that the adaptive component of SEAHF is coupled to the measured frequency content of the input image. The observed relationship between spectral energy ratio and cutoff frequency is consistent with the formulation in Section 2.4 and provides the basis for the subsequent visual and quantitative evaluation of the enhancement results.

3.2. Visual Comparison of Enhanced Images

To qualitatively evaluate the proposed method, representative astronomical images from the SDSS, DECaLS, and Pan-STARRS datasets were enhanced using CLAHE, CHF, LIME, and the proposed SEAHF. Figure 3.2 presents the visual comparison between the original images and the enhancement results obtained by each method.

As shown in Figure 3.2, each enhancement method produces distinct visual characteristics. CLAHE increases local contrast and makes spiral structures and other faint details more apparent than in the original images. However, the stronger local contrast enhancement also makes background fluctuations more visible, particularly in the SDSS and DECaLS examples, resulting in a grainier appearance in low-intensity regions. These observations are consistent with the local contrast enhancement behavior of CLAHE.

CHF produces a smoother appearance by attenuating low-frequency illumination components while moderately enhancing higher-frequency components. The resulting background is generally more homogeneous than that obtained with CLAHE. However, some fine structures remain less pronounced, particularly when a fixed cutoff does not correspond well to the spectral characteristics of the input image. This behavior illustrates the limitation of applying a single cutoff frequency to images with different spectral compositions.

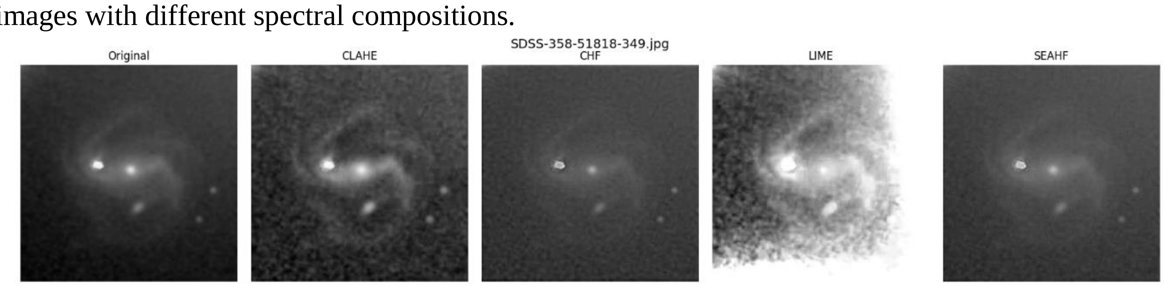

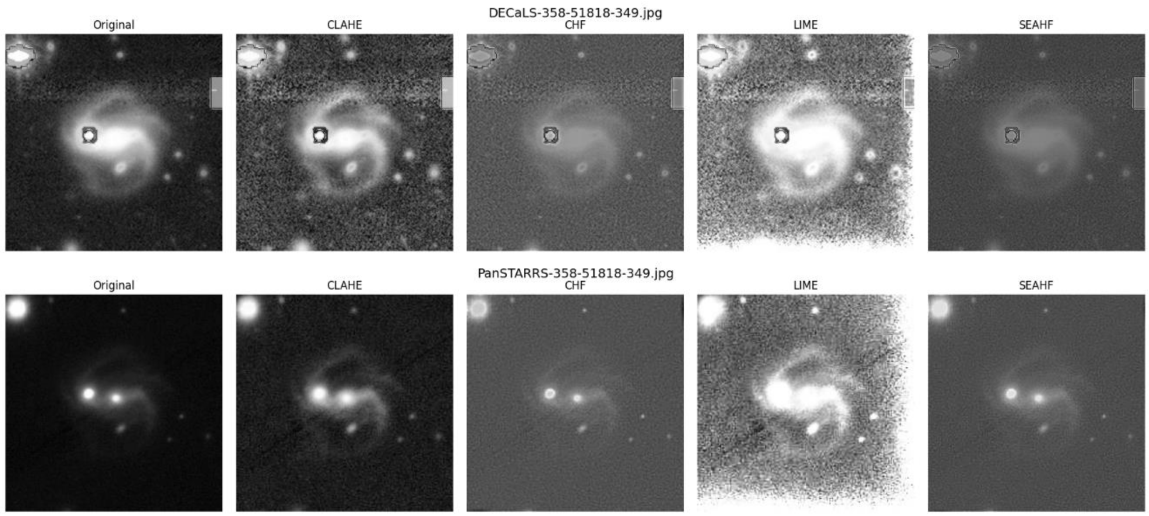

Figure 3.2. Visual comparison of enhancement results for representative images from the SDSS, DECaLS, and Pan-STARRS datasets.

LIME produces the strongest apparent brightness enhancement among the compared methods. This increases the visibility of faint regions, but in several representative images, particularly from DECaLS and Pan-STARRS, the stronger illumination enhancement is accompanied by reduced local contrast in bright regions and more visible background fluctuations. The resulting appearance suggests that increasing overall brightness does not necessarily preserve the relative visual balance between astronomical structures and their background.

Compared with the benchmark methods, SEAHF produces a more moderate enhancement of the galaxy structures while maintaining a relatively uniform background. The enhanced images retain the major structural features visible in the original images without the pronounced background amplification observed with CLAHE or the stronger brightness increase observed with LIME. Compared with CHF, the use of an image-dependent cutoff allows the filtering response to vary according to the spectral characteristics of each input image rather than applying the same frequency transition to all images.

The visual differences can therefore be interpreted in terms of the different enhancement mechanisms. CLAHE emphasizes local intensity differences, which can simultaneously strengthen structures and background fluctuations. LIME emphasizes illumination enhancement, which can improve visibility in dark regions but may also produce excessive brightness. CHF and SEAHF both operate within the homomorphic filtering framework; however, CHF uses a fixed cutoff, whereas SEAHF adjusts the cutoff according to the measured spectral energy ratio. The representative results suggest that this adaptive selection provides a more balanced visual response across the three survey images.

The visual comparison provides qualitative evidence of the effect of adaptive cutoff selection, but it does not by itself establish superiority in all aspects of image quality. The quantitative evaluation in the following sections is therefore used to assess structural preservation, illumination-order preservation, information content, and computational cost more objectively.

3.3. Quantitative Evaluation Across Datasets

The quantitative evaluation across the SDSS, DECaLS, and Pan-STARRS datasets is summarized in Tables 3.1–3.3. The proposed SEAHF was compared with CLAHE, Conventional Homomorphic Filtering (CHF), and Low-Light Image Enhancement via Illumination Map Estimation (LIME) using

SSIM, entropy, LOE, and processing time. The results show that the relative performance of the enhancement methods varies across evaluation criteria and datasets, with SEAHF exhibiting its most consistent advantage in illumination-order preservation as measured by LOE.

Table 3.1. Quantitative evaluation results for the SDSS dataset

Method	SSIM	Entropy	LOE	Time (s)
CLAHE	0.5101	5.2953	318069.1	0.001504
CHF	0.3393	5.1087	601150.3	0.009892
LIME	0.103	7.4329	1562677	1.043103
SEAHF	0.3784	5.0311	315280.1	0.009775

For the SDSS dataset, CLAHE achieved the highest SSIM (0.5101), followed by SEAHF (0.3784), CHF (0.3393), and LIME (0.1030). In terms of entropy, LIME produced the highest value (7.4329), while CLAHE (5.2953), CHF (5.1087), and SEAHF (5.0311) produced relatively similar values. The higher entropy obtained by LIME indicates a broader intensity distribution, but the corresponding visual result in Figure 3.2 also shows stronger background amplification. Therefore, the entropy result should be interpreted together with the illumination-preservation and visual characteristics of the enhanced image rather than as an independent indicator of enhancement quality.

For illumination preservation, SEAHF achieved the lowest LOE on SDSS (315280.1), slightly lower than CLAHE (318069.1) and substantially lower than CHF (601150.3) and LIME (1562677). The small difference between SEAHF and CLAHE in LOE, despite CLAHE obtaining higher SSIM, indicates that the two methods emphasize different aspects of enhancement: CLAHE provides stronger local structural contrast, whereas SEAHF produces an enhancement that more closely preserves the relative lightness ordering of the original image. SEAHF required an average processing time of 0.0098 s, which was nearly identical to CHF (0.0099 s) and considerably lower than LIME (1.0431 s).

Table 3.2. Quantitative evaluation results for the DECaLS dataset

Method	SSIM	Entropy	LOE	Time (s)
CLAHE	0.5971	7.2217	924929.9	0.001042
CHF	0.6766	6.566	763511.4	0.009747
LIME	0.2625	7.4023	2034591	0.913304
SEAHF	0.6315	6.6391	568142.5	0.009591

For the DECaLS dataset, CHF achieved the highest SSIM (0.6766), while SEAHF obtained 0.6315, followed by CLAHE (0.5971) and LIME (0.2625). In terms of entropy, LIME again produced the highest value (7.4023), while SEAHF (6.6391) was slightly higher than CHF (6.5660) and lower than CLAHE (7.2217). The relatively high SSIM of CHF indicates that the fixed-cutoff homomorphic filter can preserve structural similarity effectively for this dataset, but it does not provide the same level of illumination-order preservation achieved by SEAHF.

SEAHF achieved the lowest LOE on DECaLS (568142.5), compared with CHF (763511.4), CLAHE (924929.9), and LIME (2034591). This result is particularly relevant to the proposed adaptive mechanism because the improvement over CHF occurs while the two methods use the same homomorphic filter parameters and differ primarily in their cutoff-frequency selection. The processing time of SEAHF (0.0096 s) was also nearly identical to CHF (0.0097 s) and substantially lower than LIME (0.9133 s). Thus, the adaptive cutoff calculation does not introduce a noticeable computational burden relative to conventional homomorphic filtering in this experiment.

Table 3.3. Quantitative evaluation results for the Pan-STARRS dataset

Method	SSIM	Entropy	LOE	Time (s)
CLAHE	0.6782	7.0735	1131791	0.000965
CHF	0.7342	6.4927	828315.2	0.009787
LIME	0.4693	7.0497	1962238	0.822978
SEAHF	0.7042	6.5236	714288.8	0.008755

For the Pan-STARRS dataset, CHF again achieved the highest SSIM (0.7342), followed by SEAHF (0.7042), CLAHE (0.6782), and LIME (0.4693). CLAHE obtained the highest entropy (7.0735), whereas SEAHF (6.5236) remained close to CHF (6.4927) and below LIME (7.0497). As in the other datasets, the method with the highest entropy was not necessarily the method with the best illumination preservation, reinforcing the need to interpret the metrics jointly.

SEAHF again achieved the lowest LOE on Pan-STARRS (714288.8), compared with CHF (828315.2), CLAHE (1131791), and LIME (1962238). The same ordering of LOE observed across all three datasets indicates a consistent advantage of SEAHF in preserving the relative lightness structure of the input images. Its average processing time was 0.0088 s, slightly faster than CHF (0.0098 s) and substantially faster than LIME (0.8230 s).

Across the three datasets, the most consistent result is therefore the lower LOE obtained by SEAHF, whereas the highest SSIM varies between CLAHE and CHF. SEAHF also maintains entropy values close to those of CHF while avoiding the substantially higher entropy associated with LIME, which in the visual results was accompanied by stronger background and brightness enhancement. The processing times of SEAHF and CHF remain very close across all three datasets, indicating that the additional spectral-energy analysis required for adaptive cutoff estimation introduces only a small computational overhead in the evaluated setting.

These results suggest that the principal contribution of SEAHF is not to maximize every individual image-quality metric, but to provide a consistent balance between structural preservation, illumination-order preservation, and computational efficiency. In particular, the lower LOE across all three datasets is consistent with the intended role of the adaptive cutoff mechanism, while the competitive SSIM values indicate that this improvement in illumination preservation is not achieved through a substantial loss of structural similarity.

3.4. Overall Performance and Trade-off Analysis

The overall quantitative performance across the 60 astronomical images is summarized in Table 3.4. The results provide a cross-dataset view of the trade-offs among structural similarity, image information content, illumination-order preservation, and computational cost.

Table 3.4. Overall quantitative evaluation

Method	SSIM	Entropy	LOE	Time (s)
CLAHE	0.5951	6.5302	791596.8	0.00117
CHF	0.5834	6.0558	730992.3	0.009809
LIME	0.2782	7.295	1853169	0.926462
SEAHF	0.5714	6.0646	532570.5	0.009374

Based on Table 3.4, CLAHE achieved the highest average SSIM (0.5951), followed by CHF (0.5834) and SEAHF (0.5714), while LIME obtained the lowest value (0.2782). The relatively small difference between SEAHF and the two highest-performing methods indicates that the adaptive cutoff mechanism preserves a level of structural similarity comparable to the conventional and local contrast enhancement approaches evaluated in this study.

Regarding image information content, LIME achieved the highest average entropy (7.295), whereas SEAHF (6.0646) and CHF (6.0558) produced very similar values. CLAHE obtained an intermediate value of 6.5302. The higher entropy of LIME indicates a broader intensity distribution, but the visual comparison in Figure 3.2 shows that this increase is accompanied in several cases by stronger brightness enhancement and background amplification. Thus, entropy alone does not necessarily correspond to better preservation of astronomical image appearance or illumination relationships.

SEAHF achieved the lowest average LOE (532570.5), followed by CHF (730992.3), CLAHE (791596.8), and LIME (1853169). Compared with CHF and CLAHE, SEAHF reduced the average LOE by approximately 27.1% and 32.7%, respectively. This result is consistent with the intended role of the adaptive cutoff mechanism: the cutoff frequency is adjusted according to the relative spectral composition of each input image, allowing the filtering transition to vary between images rather than applying a single fixed transition. In this framework, the spectral energy ratio provides an image-dependent basis for determining the frequency range over which the homomorphic response changes from low-frequency attenuation toward high-frequency amplification. Such adaptation can reduce the likelihood of applying the same frequency transition to images with different spectral compositions, which may contribute to the observed preservation of relative lightness relationships reflected by the lower LOE. However, this interpretation should be considered as an empirical association rather than a direct causal proof, since the present study does not isolate the effect of the cutoff frequency through a systematic sensitivity or ablation analysis.

In terms of computational efficiency, CLAHE remained the fastest method with an average processing time of 0.00117 s per image. SEAHF required 0.009374 s, which was close to the processing time of CHF (0.009809 s) and substantially lower than LIME (0.926462 s). The small difference between SEAHF and CHF indicates that the additional spectral-energy calculation and adaptive cutoff estimation do not substantially increase the computational cost of the homomorphic filtering framework under the evaluated experimental conditions.

Taken together, the results indicate that the main advantage of SEAHF lies in its balance across the evaluated criteria rather than in achieving the best value for every individual metric. CLAHE provides the highest structural similarity and the lowest computational cost, while LIME produces the highest entropy but also the highest LOE and substantially longer processing time. CHF provides strong structural similarity and similar computational efficiency to SEAHF, but its fixed cutoff results in higher LOE. SEAHF, in contrast, achieves the lowest LOE while maintaining competitive SSIM, entropy close to CHF, and processing time comparable to CHF.

This pattern is particularly relevant to the objective of the proposed method. The adaptive mechanism is designed primarily to make the cutoff frequency responsive to image-dependent spectral characteristics, rather than to optimize a single image-quality metric. The consistently lower LOE observed across the three datasets therefore provides the strongest empirical indication of the benefit of the proposed adaptive cutoff strategy, while the comparable SSIM and computational cost suggest that the improvement in illumination-order preservation is obtained without a substantial loss of structural similarity or an appreciable computational overhead.

The present evaluation nevertheless has several limitations. The results are based on average performance over 60 selected galaxy images from three survey sources, and variability or statistical significance across individual images was not analyzed. In addition, the current study evaluates image-enhancement quality only and does not assess the effect of SEAHF on downstream astronomical tasks such as source detection, segmentation, or classification. The linear mapping used for cutoff estimation and the median-based frequency partition were also not compared systematically with alternative formulations. These aspects are therefore outside the scope of the present initial evaluation and provide directions for subsequent investigation.

4. CONCLUSION

This study proposed an Spectral Energy-Based Adaptive Homomorphic Filtering (SEAHF) method for astronomical image enhancement by estimating the cutoff frequency from the spectral energy ratio between low- and high-frequency components. The proposed method retains the conventional Gaussian homomorphic filtering framework while adapting the cutoff frequency to the spectral characteristics of each input image.

Experimental results on 60 astronomical images from the SDSS, DECaLS, and Pan-STARRS datasets showed that SEAHF consistently achieved the lowest LOE across the three evaluated datasets, while maintaining competitive SSIM and entropy values and processing times comparable to conventional homomorphic filtering. Although SEAHF did not achieve the highest performance for every individual metric, the results indicate a favorable balance between structural preservation, illumination-order preservation, and computational efficiency. The consistently lower LOE provides the strongest empirical evidence of the benefit of the proposed adaptive cutoff mechanism within the evaluated experimental setting.

The findings should be interpreted within the scope of this initial evaluation, which is based on 60 selected galaxy images from three astronomical survey sources. The study does not yet provide statistical significance analysis, systematic comparison of alternative cutoff mappings or frequency-partition criteria, or evaluation of downstream astronomical tasks. Future work may therefore investigate alternative spectral descriptors and nonlinear cutoff mappings, sensitivity to different frequency-partition strategies, and broader datasets containing other astronomical object types such as nebulae, star clusters, and deep-sky images. The integration of SEAHF into downstream astronomical image analysis, including source detection, segmentation, and classification, also represents a potential direction for further investigation.

CONFLICT OF INTEREST

The authors declare that they have no known competing financial interests or personal relationships that could have appeared to influence the work reported in this paper.

REFERENCES

[1] Almeida, A. et al., 2023. The Eighteenth Data Release of the Sloan Digital Sky Surveys: Targeting and First Spectra from SDSS-V. *The Astrophysical Journal Supplement Series*, Vol. 267, No. 2, 44.
[2] Chambers, K. C. et al., 2016. The Pan-STARRS1 Surveys. *arXiv*, arXiv:1612.05560.
[3] Dey, A. et al., 2019. Overview of the DESI Legacy Imaging Surveys. *The Astronomical Journal*, Vol. 157, No. 5, 168.
[4] Fan, C.N. & Zhang, F.Y., 2011. Homomorphic Filtering Based Illumination Normalization Method for Face Recognition. *Pattern Recognition Letters*, Vol. 32, No. 10, 1468–1479.
[5] Fan, Y., Zhang, L., Guo, H., Hao, H. & Qian, K., 2020. Image Processing for Laser Imaging Using Adaptive Homomorphic Filtering and Total Variation. *Photonics*, Vol. 7, No. 2, 30.
[6] Gonzalez, R. C. & Woods, R. E., 2018. *Digital Image Processing*. Pearson Education, Harlow.
[7] Guo, X., Li, Y. & Ling, H., 2017. LIME: Low-Light Image Enhancement via Illumination Map Estimation. *IEEE Transactions on Image Processing*, Vol. 26, No. 2, 982–993.
[8] Hong, Y. et al., 2024. Optimizing Image Processing for Modern Wide Field Surveys. *Frontiers in Astronomy and Space Sciences*, Vol. 11, 1402793
[9] Jain, A. K., 1989. *Fundamentals of Digital Image Processing*. Prentice Hall, New Jersey.

[10] Jiang, H., Luo, A., Han, S., Fan, H. & Liu, S., 2023. Low-Light Image Enhancement with Wavelet-based Diffusion Models. *ACM Transactions on Graphics*, Vol. 42, No. 6, 250.

[11] Khlamov, S., 2024. Astronomical Image Processing by the Lemur Software. *Proceedings of the 2024 6th Asia Conference on Machine Learning and Computing*, 139-145

[12] Lei, M., Li, H., Lu, X. & Shen, D., 2025. Diffusion Generation with Homomorphic Filtering for Remote Sensing Thin Cloud Removal. *Geo-Spatial Information Science*, 1–14.

[13] Liu, G., 2022. A Combined Method of Image Enhancement Based on Self-Adaptive Median Filtering and Homomorphic Filtering Algorithm. *Proceedings of the 3rd Asia-Pacific Conference on Image Processing*, *Electronics and Computers 2022*, 285–289.

[14] Luo, Z. et al., 2024. Cross-Survey Image Transformation: Enhancing SDSS and DECaLS Images to Near-HSC Quality. *arXiv*. arXiv:2410.20025v2.

[15] Schirninger, C. et al., 2025. Deep Learning Image Burst Stacking to Reconstruct High Resolution Astronomical Images. *Astronomy & Astrophysics*, Vol. 695, A126.

[16] Singh, K., Kapoor, R. & Sinha, S. K., 2015. Enhancement of Low Exposure Images via Recursive Histogram Equalization Algorithms. *Optik*, Vol. 126, No. 20, 2619–2625.

[17] Wang, S., Zheng, J., Hu, H.-M. & Li, B., 2013. Naturalness Preserved Enhancement Algorithm for Non-Uniform Illumination Images. *IEEE Transactions on Image Processing*, Vol. 22, No. 9, 3538–3548.

[18] Wang, Z., Bovik, A. C., Sheikh, H. R. & Simoncelli, E. P., 2004. Image Quality Assessment: From Error Visibility to Structural Similarity. *IEEE Transactions on Image Processing*, Vol. 13, No. 4, 600–612.

[19] Xiao, W. et al., 2019. Adaptive Frequency Filtering Based on Convolutional Neural Networks in Off-Axis Digital Holographic Microscopy. *Biomedical Optics Express*, Vol. 10, No. 4, 1613–1626.

[20] Xu, G., Huang, W., Jia, W., Li, J., Gao, G. & Qi, G.-J., 2026. Diffusion-based Laplacian Frequency-aware Network for Low-Light Image Enhancement. *Pattern Recognition*, Vol. 175, 113060.

[21] Xu, X., Wang, R. & Lu, J., 2023. Low-Light Image Enhancement via Structure Modeling and Guidance. *Proceedings of the IEEE/CVF Conference on Computer Vision and Pattern Recognition (CVPR)*, 12685–12695.

[22] Xue, M., He, J., Wang, W. & Zhou, M., 2024. Low-light Image Enhancement via CLIP-Fourier Guided Wavelet Diffusion. *arXiv*, arXiv:2401.03788.

[23] Zhao, R., Lam, K.-M. & Lun, D. P. K., 2020. Enhancement of a CNN-Based Denoiser Based on Spatial and Spectral Analysis. *arXiv*, arXiv:2006.15517.